Nanoscale

PAPER

View Article Online
View Journal | View Issue

Cite this: *Nanoscale*, 2023, **15**, 3864

Nitrogen- and sulfur-doped graphene quantum dots for chemiluminescence†‡

Xiaoli Qin, §[a,b] Ziying Zhan,§[a] Ruizhong Zhang,§[a,c] Kenneth Chu,[a] Zackry Whitworth[a] and Zhifeng Ding *[a]

Graphene quantum dots (GQDs), as one of the most promising luminescent nanomaterials, have been receiving increasing attention in various applications. However, it is still a challenge to improve their chemiluminescence (CL) quantum efficiency. Herein, the CL emissions of nitrogen- and sulfur-doped GQDs (NS-GQDs), nitrogen-doped GQDs (N-GQDs) and undoped GQDs synthesized through one-pot high-temperature pyrolysis are investigated in their chemical reactions with bis(2-carbopentyloxy-3,5,6-trichlorophenyl) oxalate (CPPO) and hydrogen peroxide (H_2O_2). A bright blue emission, and yellowish green and yellowish white light from NS-GQDs, N-GQDs and GQDs can be observed, respectively, in the mixture solutions with CPPO and H_2O_2. For the first time, spooling CL spectroscopy was used to investigate the CL reaction mechanisms, illuminant decays and the absolute CL efficiencies of these three GQD systems. Compared with the same system of undoped GQDs, it has been found that the NS-GQDs not only present slower illuminant decay, but also display an absolute CL quantum efficiency of 0.01%, 5-fold enhancement, due to the increase in N and S doping for a well-defined band gap energy. Moreover, three peak wavelengths attributed to intrinsic emission at 425 nm, aggregation-induced emission (AIE) at 575 nm and S-doped emissive surface states at 820 nm are observed for the first time in the NS-GQD system. The CL spectrum of N-GQDs displays two emission peaks at 395 and 575 nm attributed to intrinsic emission and AIE, whereas the CL spectrum of undoped GQDs demonstrates 500 nm and 600 nm peak wavelengths attributed to core emission and AIE. Absolute CL quantum efficiencies from these emissions at these various peaks can be determined quantitatively. This study provides guidance on tuning the surface states of GQD for more conducive injection of electrons and holes, facilitating the production of CL emission, which is beneficial for promoting the development of optical, bioassay and energy conversion applications.

Received 23rd December 2022,
Accepted 19th January 2023

DOI: 10.1039/d2nr07213k

rsc.li/nanoscale

1 Introduction

Carbon quantum dots (CQDs), as a small carbon nanoparticle with size less than 10 nm in diameter, have attracted much attention over the last few decades due to their luminescence properties and nanoscale size.[1–4] Graphene quantum dots (GQDs), as a subset of CQDs, are generally derived from graphene oxide or graphene and exhibit chemical and physical properties similar to those of graphene.[5–10] GQD synthesis can be easily achieved through a top-down or bottom-up approach from various precursors.[6–8,11] Because of their fascinating chemical properties, excellent optical features, attractive catalytic performance, good water dispersity and chemical stability, GQDs exhibit great potential in application fields such as catalysis,[12,13] energy,[14] sensing[15] and biomedicine.[16] The unique optical properties of GQDs are related to their shell–core composition, which can be optimized by modifying the functional groups located at the edge.[14] Various luminescence mechanisms of GQDs, including fluorescence and phosphorescence, have been proposed and provide great opportunities in wide applications.[3] Moreover, to explore the electrochemiluminescence (ECL) mechanisms of the GQDs, our group synthesized different GQDs, including near-infrared (NIR)-emitting GQDs, to investigate the ECL performance.[7,8]

Chemiluminescence (CL) is a light-emitting phenomenon produced by chemical reactions[17–19] and has been widely used in cold light sources, biological analysis, chemical detection

[a]*Department of Chemistry, Western University, London, Ontario N6A 5B7, Canada. E-mail: zfding@uwo.ca*
[b]*College of Chemistry and Materials Science, Hunan Agricultural University, Changsha 410128, China*
[c]*Tianjin Key Laboratory of Molecular Optoelectronic Sciences, Department of Chemistry, School of Science, Tianjin University, Tianjin 300072, China*
†Dedicated to the home university, Southeast University, for its great contribution to high-quality personnel training on occasion of its 120th anniversary.
‡Electronic supplementary information (ESI) available. See DOI: https://doi.org/10.1039/d2nr07213k
§These authors equally contributed to this work.

and so on.[20,21] The CL reaction of GQD originates from the clear energy separations of the surface states. Hence, the energy gaps between the lowest unoccupied molecular orbital (LUMO) and the highest occupied molecular orbital (HOMO) levels in the surface states of GQD are more conducive to the injection of electrons and holes, facilitating the production of CL emissions.[22] It is well known that the energy gap of the surface states correlates with the size of GQD, the extent of the π-electron system and surface chemistry.[23] Generally, higher surface oxidation of the GQD causes more surface defects and reduces the energy levels. For example, the C–OH and C–O–C groups on the surface of GQD can often introduce some new energy gaps between n–π* gaps, resulting in lower excitation energies for surface state transitions than those for the original n–π* transitions.[24] Moreover, Kang *et al.* have also proved that the doping of N- and/or S-made CQDs has a lower band gap energy than that of CQDs.[25] Prato *et al.* have summarized the synthesis conditions regulating the degree of carbonization and graphitization (or the final structure) for bottom-up synthesized carbonaceous nanoparticles.[26]

Energy transfer CL or CL resonance energy transfer (CRET) has been rapidly developed in the CL-based excitation of fluorophores, such as 1,2-dioxetane-based CL reactions,[27,28] which can greatly improve the efficiency of CL and is also a major breakthrough in the field of CL research.[27] In the peroxyoxalate-based CL (PO-CL) reactions, QDs can achieve intensified and prolonged luminescence processes more than traditional fluorophores when they undergo the CRET reaction.[29] Shan's group established temperature-dependent CL imaging based on the temperature-dependent CL emission of carbon nanodots in the chemical reaction of hydrogen peroxide (H_2O_2) and bis(2,4,5-trichloro-6-carbopentoxyphenyl) oxalate (CPPO).[21] Chen *et al.* proved that a system composed of bis(2,4,6-trichlorophenyl) oxalate (TCPO), fluorescein and H_2O_2 can enhance the CL of graphene oxide QDs (GOQDs).[30] However, studies of N and S doping effects on GQD PO-CL have not been reported to date.

Therefore, this work aims to study the PO-CL reactions of nitrogen- and sulfur-doped GQDs (NS-GQDs), nitrogen-doped GQDs (N-GQDs) and undoped GQDs, and determine their corresponding absolute CL efficiencies (Scheme 1). With the naked eye, it can be clearly seen that NS-GQD, N-GQD and GQD exhibit blue, green and yellowish white CL emissions, respectively, in a solution mixture containing CPPO, H_2O_2 and sodium salicylate. For the first time, the spooling CL spectroscopy was utilized to study the CL mechanisms, illuminant decay and the absolute CL efficiencies of these three NS-GQD, N-GQD and GQD systems. With NS-GQDs as the CL emitter, the CL spectrum presents three peak wavelengths attributed to intrinsic emission, aggregation-induced emission (AIE) greatly discovered and introduced by Tang *et al.* for various molecules and materials[31–33] and S-doped emissive surface states. Compared with the N-GQD and undoped GQD systems, the NS-GQD system displays a slower illuminant decay and a higher CL efficiency due to the N and S doping, leading to a large degree of property alternation.

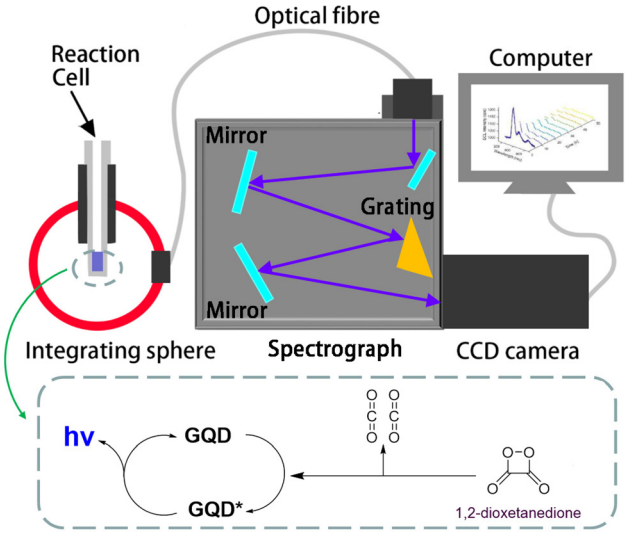

Scheme 1 Schematic overview of the CL instrumentation and CL generation of GQDs.

2 Experimental section

2.1 Materials and reagents

Sodium salicylate (≥99.5%), bis(2-carbopentyloxy-3,5,6-trichlorophenyl) oxalate (CPPO, ≥96.5%) and ethyl acetate (≥99.5%) were purchased from Sigma-Aldrich Canada and used as received. Acetonitrile (≥99.5%) and hydrogen peroxide (H_2O_2, 30%) were provided by Thermo Fisher Scientific (Canada) and used as received.

2.2 CL spectroscopy

All measurements were conducted inside a cylindrical glass tube. The CL spectra of GQDs were collected using a 6 inch integrating sphere (Labsphere, North Sutton, NH, USA) and a set of a charge-coupled device (CCD) camera (iDUS401a-BR-DD, Andor Technologies, Belfast, UK) cooled at −65 °C and a spectrograph (Acton SP2300i, Teledyne Princeton Instruments – Massachusetts, USA), as shown in Scheme 1. Light emissions were collected completely by the integrating sphere diffusing homogeneously and sending a certain amount of light to the spectrograph through an optical fibre. Light collection is not dependent on the CL cell geometry, as long as it is in the integrating sphere. Calibration of the spectroscopy wavelength on the set of the spectrograph and the CCD camera was performed using a mercury–argon source (model HG-1, Ocean Insight, Orlando, FL, USA).[34] All accumulation emission spectra reported in this work have been baseline-corrected by numerical subtraction of an identical duration background scan, and intensity normalized to allow for a meaningful comparison. The spectrograph and CCD camera set were calibrated using an Ocean Insight USB2000+ spectrometer with a calibration lamp (LS-1-CAL-int) along with the integrating sphere. In total, five calibration points were collected by varying the running time of the lamp with 1, 2, 3, 4

and 5 s, respectively. These measurements were then repeated on the spectrograph–CCD camera set to correlate to the optical power readings. An optical density filter was used to reduce the radiant power of the standard lamp to a scale appropriate for the calibration procedures. The measured CL spectra were interpolated to derive 2048 wavelength pixels with an interval value of 0.38 nm in a wavelength range between 341.21 and 1029.64 nm and ultimately converted from counts to power values in μW nm^{-1}, which were further converted to numbers of photons. The total photons were obtained by integration of the light quanta–wavelength curves with the assistance of custom programs in MATLAB software (version 2021b, MathWorks Inc., Natick, MA, USA) developed in our group, similar to those for determining absolute electrochemiluminescence efficiencies.[8,35,36]

2.3 Synthesis and characterization of the GQDs, N-GQDs and NS-GQDs

Undoped GQDs, N-GQDs and NS-GQDs were synthesized *via* a one-pot high-temperature pyrolysis method.[7] Typically, 2.0 g of citric acid without or with 0.6 g of L-cysteine was first mixed in a 50 mL round-bottom flask and then heated at 240 °C using a heating mantle. The mixture fully liquidated in about 2 min. Subsequently, the liquid color changed from colorless to pale yellow and finally to orange in about 4 min. The obtained liquid was then dissolved in 20 mL of ultrapure water. The resulting orange solution was further dialyzed for 8 h using a dialysis bag with a molecular weight cutoff (MWCO) of 1000 Da against ultrapure water for purification. Finally, the product in the dialysis bag was dried through a freeze dryer. In addition, 2.0 g of citric acid with 0.6 g of L-alanine was used to synthesize the N-GQDs through the abovementioned steps. The undoped GQDs were prepared using 2.0 g of citric acid as the pyrolysis precursor.

3 Results and discussion

3.1 CL observations of NS-GQDs, N-GQDs and GQDs

In this work, NS-GQDs, N-GQDs and GQDs were easily synthesized *via* a one-pot high-temperature pyrolysis method and were characterized as we reported elsewhere.[7] The PL quantum yields of NS-GQDs, N-GQDs and GQDs were determined to be 46.8%, 2.3% and 0.5%, respectively. Fig. 1 demonstrates that CL emissions can be observed in a dark room from NS-GQDs, N-GQDs and GQDs in a concentration of 3 mg mL^{-1} in the presence of 20 mg mL^{-1} CPPO, 15% H_2O_2 and 1 mg mL^{-1} sodium salicylate as the base catalyst. A blue glow emission of NS-GQDs, a yellowish green emission of N-GQDs and a yellowish white light of GQDs were observed by the naked eye, respectively, which lasted up to 50 s. The reaction mechanism of the GQDs chemiexcited by CPPO and hydrogen peroxide is shown in the inset of Scheme 1 and detailed in Fig. S1.‡ In the chemical reactions as illustrated in Scheme 1, CPPO reacts with H_2O_2 in the presence of sodium salicylate acting as a base catalyst and produces oxalyl chloride. The oxalyl chloride as an unstable intermediate is quickly converted into 1,2-dioxetanedione, another high-energy intermediate, which subsequently decomposes into two CO_2 molecules and releases high energy. Finally, the three types of GQDs absorb the released energy and then generate CL emissions.[37] These CL emissions are very fast and obvious luminous phenomena can be seen with the naked eye. It has been hypothesized that the differences in light emissions among NS-GQDs, N-GQDs and GQDs mainly result from the combining effects of intrinsic blue emissions from the dots, graphene aggregation-induced emission (AIE)[32] and surface state green/red emissions with sulfur functional groups and surface energy traps.[7,24,38]

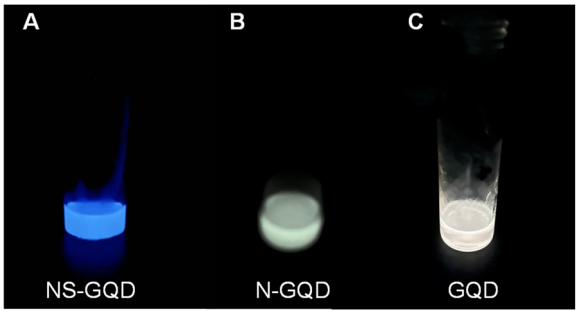

Fig. 1 Digital photographs of the NS-GQDs (A), N-GQDs (B) and GQDs (C) CL reactions. Reaction conditions: 3 mg mL^{-1} of each GQDs, 20 mg mL^{-1} CPPO, 15% H_2O_2 and 1 mg mL^{-1} sodium salicylate.

3.2 CL spectroscopy of NS-GQDs, N-GQDs and GQDs

Next, the CL mechanisms and the associated efficiencies of the NS-GQD, N-GQD and GQD systems were further explored by CL spectroscopy. Scheme 1 displays the instrumentation required to perform the CL spectroscopic measurements. The CL spectrum was acquired by the set of an Acton SP2300i spectrograph and an Andor CCD camera along with a 6-inch integrating sphere. The cylindrical glass tube CL cell was placed inside the integrating sphere so that the total CL emission was dispersed homogeneously and collected proportionally through an optical fibre connecting the sphere port and the spectrograph (Scheme 1). Spooling CL spectroscopy, which takes CL spectra at a certain accumulated time interval during the emission process, involving the real-time monitoring of CL, was developed and employed for the first time to reveal the kinetics of the CL reactions, which is similar to that of spooling ECL spectroscopy.[34] Fig. 2 shows the spooling CL spectra of the NS-GQD system at a time interval of 5 s with a concentration of 0.2 mg mL^{-1} in the presence of 0.17% H_2O_2, 3.7 mg mL^{-1} CPPO and 2.0 mg mL^{-1} sodium salicylate in an 80% ethyl acetate and 20% acetonitrile solution. Three emission peaks can be observed at 425 nm, 575 nm and 820 nm. The predominant emission band centered at around 425 nm matches the PL emission of NS-GQDs centered at 430 nm (blue photoluminescence) when excited at 350 nm (Fig. S2‡). This intrinsic emission is our novel discovery, which has not been observed in the ECL of the same quantum dots.[7]

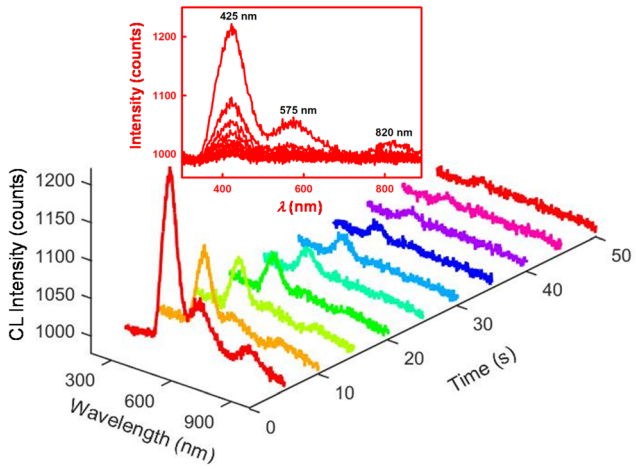

Fig. 2 Spooling CL spectra acquired at a time interval of 5 s in the presence of NS-GQD, CPPO and H_2O_2. Inset shows the 2D view of stacked spooling CL spectra demonstrating consistent shapes and peak wavelengths. Reaction conditions: adding 200 μL of 1% H_2O_2 in acetonitrile to 1 mL of an 80% ethyl acetate, 20% acetonitrile solution containing 0.2 mg mL^{-1} NS-GQDs, 3.7 mg mL^{-1} CPPO and 2 mg mL^{-1} sodium salicylate.

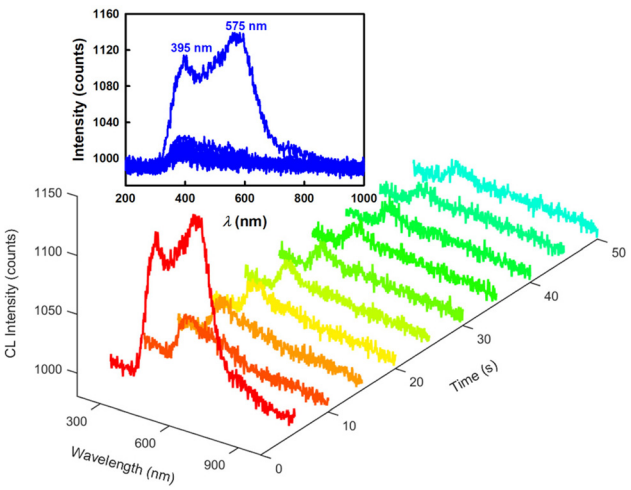

Fig. 3 Spooling CL spectra acquired at a time interval of 5 s in the presence of N-GQD, CPPO and H_2O_2. Insets show the 2D view of spooling CL spectra demonstrating constant shapes and peak wavelengths. Reaction conditions: adding 200 μL of 1% H_2O_2 in acetonitrile to 1 mL of an 80% ethyl acetate, 20% acetonitrile solution containing 0.2 mg mL^{-1} N-GQD, 3.7 mg mL^{-1} CPPO and 2 mg mL^{-1} sodium salicylate.

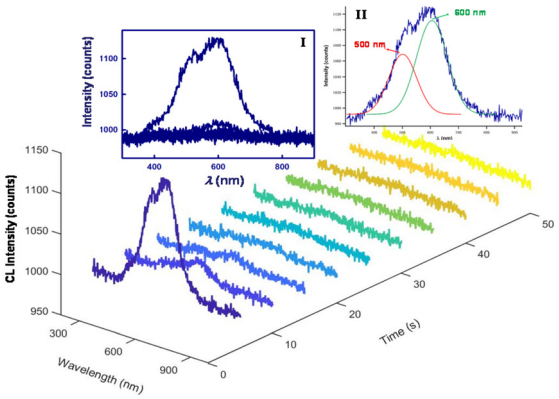

Fig. 4 Spooling CL spectra acquired at a time interval of 5 s in the presence of GQD, CPPO and H_2O_2. Insets show the (I) 2D view of spooling CL spectra demonstrating constant shapes and peak wavelengths, and (II) its curve fitting, respectively. Reaction conditions: adding 200 μL 1% H_2O_2 in acetonitrile to 1 mL of an 80% ethyl acetate, 20% acetonitrile solution containing 0.2 mg mL^{-1} GQD, 3.7 mg mL^{-1} CPPO and 2 mg mL^{-1} sodium salicylate.

Furthermore, the peak at 820 nm in Fig. S2‡ originates from the S-related surface states and is responsible for a long-wavelength CL emission in the near-infrared (NIR) region similar to the ECL emission of our N-, S-doped GQDs prepared with a hydrothermal method.[8] It is very interesting to note that the other CL emission peaks at 575 nm of the NS-GQDs are more significant than those of the ECL as we have reported elsewhere,[7] which are 145 nm red-shifted from the PL maximum at 430 nm. This can be attributed to the AIE of the graphene dots due to the utilization of a more hydrophobic solvent than water, in which the hydrophilic GQD aggregation degree is augmented.[32,33] The enhancement at 575 nm might shield the emission at around 650 nm due to the N-doped surface state emission observed in ECL in an aqueous medium,[8] as demonstrated in Fig. 3.

Fig. 3 and 4 display the spooling CL spectra of the N-GQD and undoped GQD system under the same reaction conditions as the NS-GQDs in the 80% ethyl acetate and 20% acetonitrile solvent mixture. It can be observed that the CL emission intensities of N-GQDs and undoped GQDs are relatively lower than that of NS-GQDs. As shown in Fig. 3, the CL spectra of N-GQDs display two emission peaks at 395 and 575 nm and this is why its photograph shown in Fig. 1B presents a yellowish green color. The emission maxima at 575 nm support its assignment as graphene aggregation-induced emission, which has a similar 130 nm red-shift to that at 395 nm attributed to the core band gap transition and a PL maximum at 425 nm (Fig. S3‡). There is a tiny shoulder around 790 nm, being attributed to the surface state emission. From Fig. 4, the CL spectra of GQDs also show an intensive emission covering a broad wavelength range between 350 and 800 nm and this is why its photograph shown in Fig. 1C shows a yellowish white color. The wavelength maxima at 500 nm and 600 nm support their assignment as their core emission and graphene aggregation-induced emission, which correlate to the PL maximum at 478 nm (Fig. S4‡) and the proposed AIE. No appreciable shoulder can be observed around 800 nm for the surface state emission.

It has been widely accepted that the PL mainly occurs through excitation and emission within the QD core band structure, though the electron and hole wave functions can interact strongly with the QD surface. In contrast, ECL usually depends on surface chemistry and the presence of surface

states.[39,40] The above observed results prove that the CL systems can give a wide spectrum of driving force for NS-GQDs, N-GQDs and GQDs to produce various emissions due to the concerted pathways of core structure emission, as well as AIE,[6,32] which illustrate the high energy transfer efficacy post decomposition of the high-energy intermediate 1,2-dioxetanedione to the quantum dots. In addition, the different CL emission peak wavelengths in the NS-GQD, N-GQD and the GQD systems provide insight into the red-shifted characteristic relative to their PL emission, originating from the AIE. It is possible that there are emissive traps, multiple N-, S-, C- and O-containing functional groups on the surface, generating more surface defects as active sites with different energy levels and resulting in a series of emissive traps.[7] S-containing surface states might show stronger emission than the N- and O-containing ones from the three GQDs.

Moreover, it can be found that the decays of the NS-GQD and N-GQD illuminance are significantly slower than that of undoped GQDs. In the undoped GQD system, about 98% of the total light emission disappeared after the 20 s reaction time (Fig. 4). However, in the NS-GQD and N-GQD systems, we can still see an obvious CL intensity presented at a 50 s reaction time (Fig. 2 and 3). The increase in the decay lifetimes of the NS-GQD and N-GQD is related to the increase in N and S doping, which changes the surface states and alters the emission of the defect states.[25,41]

The International Commission on Illumination (CIE) coordinate diagrams calculated according to their CL spectra of NS-GQD, N-GQD and GQD solutions are depicted in Fig. 5, showing the differences between their CL emissions, and the results are similar to those in the digital photographs presented in Fig. 1.

3.3 Absolute CL quantum efficiencies of NS-GQDs, N-GQDs and GQDs

According to previous reports on peroxyoxalate-based CL systems of organic dyes such as rubrene, rhodamine and anthracene derivatives,[37,42] the intensity of the CL reaction depends solely on the concentration of the high-energy intermediate 1,2-dioxetane, which in turn is limited by the consumption rate of the rate-limiting reagent CPPO. Thus, the CL quantum efficiency (Φ_{CL}) in Einsteins per mole is calculated from eqn (1) using eqn (2) and (3).[43,44]

$$\Phi_{CL} = \frac{\text{total number of photons}}{n_{CPPO} \times 6.02 \times 10^{23}} \times 100\% \quad (1)$$

$$E = \frac{hc}{\lambda} = J \text{ per photon } (\lambda) \quad (2)$$

$$W = \frac{J}{s} \times \frac{1}{J \text{ per photon } (\lambda)} = \frac{\text{photon } (\lambda)}{s} \quad (3)$$

where n_{CPPO} is the number of CPPO moles used in the CL reaction, c is the speed of light (3×10^8 m s^{-1}), λ is the individual photon wavelength, J is the energy of an individual photon at a wavelength of λ and h is Planck's constant (6.626×10^{-34} J s).

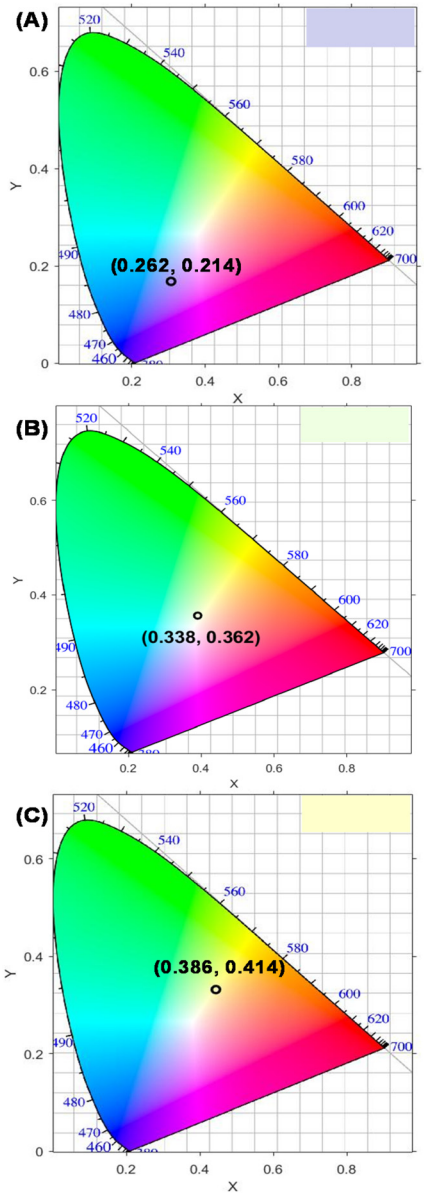

Fig. 5 CIE diagrams of CL from (A) NS-GQDs, (B) N-GQDs and (C) undoped GQDs.

The Ocean Insight USB2000+ Spectrometer (OIS) was used to normalize/calibrate our spectroscopy CCD camera as shown in Scheme 1. A measured CL spectrum (Fig. 6A) was interpolated to derive 2048 wavelength pixels with an interval value of 0.38 nm in a wavelength range between 341.21 and 1029.64 nm to match those from the OIS. The same optical fibre output from the integrating sphere illuminated with a calibration lamp was measured on both the CCD camera (Fig. S5‡) and the OIS in absolute irradiance mode (Fig. S6‡) to obtain the baseline-corrected lamp spectrum in the intensity format of counts or μW at each wavelength. A conversion curve in Fig. 6B was developed by taking the ratio of the spectrum on the CCD camera to the absolute irradiance-wavelength spectrum from the OIS, as shown in Fig. S7.‡ The μW in the

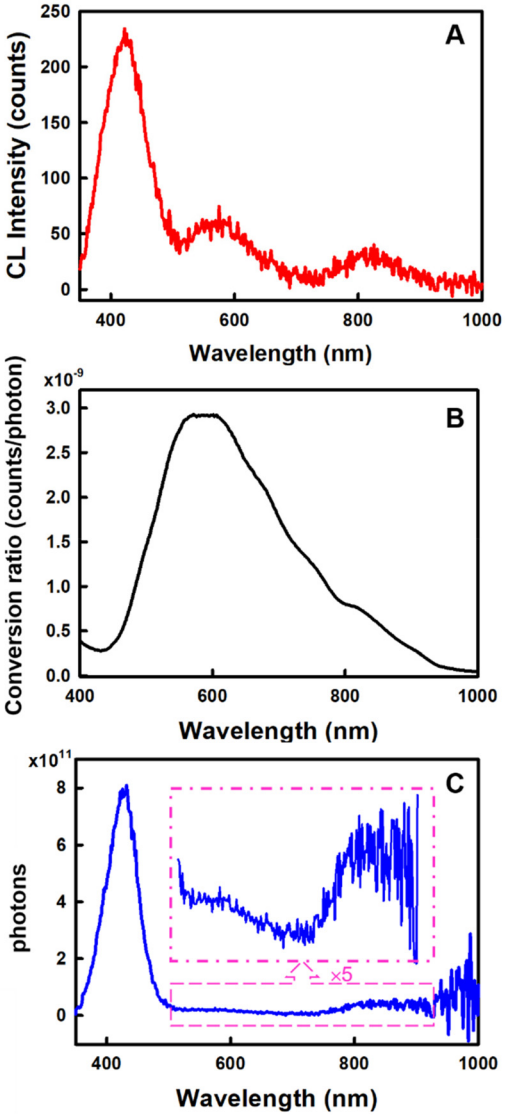

Fig. 6 (A) Background-corrected spectrum of the first 5 s lap NS-GQD CL emission. (B) The conversion curve of the counts per photon as a function of the wavelength. (C) The absolute photon response as a function of the wavelength. The second and third CL peaks are zoomed in 5 times to better display them in the inset.

conversion curve in Fig. S7‡ was further converted to the number of photons using eqn (2) and (3), relating to a photon's energy at its wavelength (λ). Fig. 6B shows the relation between final conversion ratio expressed in counts/photon as a function of the wavelength. To obtain an absolute photon response–wavelength curve (Fig. 6C), the CL spectrum measured on the CCD camera was then divided by the conversion curve as shown in Fig. 6B.

The total number of photons emitted by the system for eqn (1) can be determined by integration of the absolute photon response–wavelength curve in the appropriate wavelength range, from which a CL efficiency can be obtained straightforwardly *via* eqn (1).

The CL efficiencies of the NS-GQD, N-GQD and GQD systems were determined to be 0.01%, 0.004% and 0.002%, respectively, by adding the total number of photons to each of the spooling CL spectra as shown in Fig. 2–4. The CL efficiency of the NS-GQD system is 5-fold enhanced in comparison with that in the GQD, which is attributed to the efficient intrinsic emissive surface states favored by the sites created *via* N and S doping in the NS-GQDs.[7] That is to say, the GQDs doped with both N and S possess a more conducive injection of electrons and holes, which will obviously enhance the CL with a synergy of intrinsic emission, AIE, and emissive surface states. Very interestingly, in the NS-GQD system, the intrinsic emission, AIE, and emissive surface states contributed 77%, 4.6% and 18.4% to the total CL efficiency, respectively, demonstrating that the intrinsic emission plays a major role in this CL reaction. This illustrates that the power of our novel strategy to study GQD nanomaterial applications in various bioassays is anticipated from these GQDs. It is unlikely that other impurities caused the luminescence since they would not form the luminescent motifs. It is possible that other impurities could influence the electric and electronic properties as reported in the literature.[45,46]

Compared with traditional measurements,[47,48] utilizing the integrating sphere can collect all the light emitted and improve the collection efficiency greatly, assisting the spectrometer in measuring all the photons. For either non-standardized or standardized experimental conditions, the linearity check and calibration of instrument are always important in determining the absolute quantum efficiencies. This is because each detection system has its own background signal level due to dark photocurrents in the detector, background light, contamination of solution and other sources, which may affect the measurement of the luminescence intensity.[49] Thus, this work may also provide a suitable CL efficiency measurement for other relative luminescent systems.

4 Conclusions

In summary, a new approach for the CL emission of the GQDs, which extracts the energy released by the exothermic reaction to produce light, has been developed. Simply, CPPO reacts with H_2O_2 in the presence of a base and produces an unstable intermediate, which is converted into another high-energy intermediate and then decomposes into CO_2, and at the same time releases energy. Finally, the GQDs absorb the released energy and generate bright light *via* the CL process. The spooling CL spectroscopy was used to investigate the CL mechanisms of the as-prepared NS-GQD, N-GQD and GQD systems. The CL spectra of the NS-GQDs display three peak wavelengths at 425 nm, 575 nm and 820 nm attributed to intrinsic emission, AIE and S-doped emissive surface states, while those of GQDs show dominant AIE. The released energy from 1,2-dioxetanedione in these two systems acts as an efficient driving force to produce CL emissions. Importantly, the results of this work demonstrate N- and S-doping derived from L-cysteine to

enhance the CL efficiency of NS-GQDs 5-fold higher than that of undoped GQDs. This provides further insight into the preparation of GQDs with desired optical features by tackling current challenges such as doping and surface states. These GQD CL systems might lead to a new avenue for the promising applications of GQDs towards bioassays and clinical analyses. For example, the GQDs can act as a label for a sandwich CL immunoassay. Due to the ultrahigh CL sensitivity, it is possible that the above CL of NS-GQDs might be a convenient probing system for imaging single reaction events as CL mapping.[50]

Author contributions

X. Q.: data curation and analysis, investigation, and writing – original draft preparation and revision; Z. Z.: data curation and some analyses, visualization, validation, and investigation; R. Z.: sample preparation and resources; K. C.: data analysis and MATLAB programing; Z. W.: experimental initialization; Z. D.: conceptualization, methodology, funding acquisition, project administration, and writing – reviewing and finalization.

Conflicts of interest

There are no conflicts to declare.

Acknowledgements

This research has been supported by the Natural Sciences and Engineering Research Council of Canada (DG RGPIN-2013-201697 (Z. D.) and RGPIN-2018-06556 (Z. D.)), the Canada Foundation of Innovation/Ontario Innovation Trust (CFI/OIT, 9040), Premier's Research Excellence Award (PREA, 2003 (Z. D.)), the Canada Institute of Photonics Innovation (2005 (Z. D.)), the Ontario Photonics Consortium (2002 (Z. D.)), the National Natural Science Foundation of China (22004034 (X. Q.)), the Natural Science Foundation of Hunan Province (China) (2020JJ5226 (X. Q.)) and the China Scholarship Council (201908430010 (X. Q.)). We also thank the Electronic Shop at the Department of Chemistry and ChemBioStores, Western University, for their quality service.

References

1 J. Zhou, C. Booker, R. Li, X. Zhou, T.-K. Sham, X. Sun and Z. Ding, *J. Am. Chem. Soc.*, 2007, **129**, 744–745.
2 K. D. Patel, R. K. Singh and H.-W. Kim, *Mater. Horiz.*, 2019, **6**, 434–469.
3 L. Zhang, X. Yang, Z. Yin and L. Sun, *Luminescence*, 2022, **37**, 1612–1638.
4 M. E. Khan, A. Mohammad and T. Yoon, *Chemosphere*, 2022, **302**, 134815.
5 M. Li, T. Chen, J. J. Gooding and J. Liu, *ACS Sens.*, 2019, **4**, 1732–1748.
6 R.-S. Juang, C.-C. Fu, C.-T. Hsieh, S. Gu, Y. Ashraf Gandomi and S.-H. Liu, *J. Mater. Chem. C*, 2020, **8**, 16569–16576.
7 R. Zhang, J. R. Adsetts, Y. Nie, X. Sun and Z. Ding, *Carbon*, 2018, **129**, 45–53.
8 L. Yang, C. R. De-Jager, J. R. Adsetts, K. Chu, K. Liu, C. Zhang and Z. Ding, *Anal. Chem.*, 2021, **93**, 12409–12416.
9 H. L. Poh, P. Šimek, Z. Sofer, I. Tomandl and M. Pumera, *J. Mater. Chem. A*, 2013, **1**, 13146–13153.
10 H. L. Poh, P. Šimek, Z. Sofer and M. Pumera, *ACS Nano*, 2013, **7**, 5262–5272.
11 Z. Gan, H. Xu and Y. Hao, *Nanoscale*, 2016, **8**, 7794–7807.
12 Z. E. Gorji, A. A. Khodadadi, S. Riahi, T. Repo, Y. Mortazavi and M. Kemell, *J. Environ. Sci.*, 2023, **126**, 408–422.
13 D. Dinda, H. Park and S. Y. Park, *J. Catal.*, 2021, **404**, 273–282.
14 A. Ghaffarkhah, E. Hosseini, M. Kamkar, A. A. Sehat, S. Dordanihaghighi, A. Allahbakhsh, C. van der Kuur and M. Arjmand, *Small*, 2022, **18**, 2102683.
15 I. A. Revesz, S. M. Hickey and M. J. Sweetman, *J. Mater. Chem. B*, 2022, **10**, 4346–4362.
16 S. Sangam, S. Jindal, A. Agarwal, B. D. Banerjee, P. Prasad and M. Mukherjee, *Biomater. Sci.*, 2022, **10**, 1647–1679.
17 Y. Liu, W. Shen and H. Cui, *Anal. Chem.*, 2019, **91**, 10614–10621.
18 Y. Fan, H. Xing, Q. Zhai, D. Fan, J. Li and E. Wang, *Anal. Chem.*, 2018, **90**, 11651–11657.
19 S. Dong, D. Wang, X. Gao, L. Fu, J. Jia, Y. Xu, B. Zhang and G. Zou, *Anal. Chem.*, 2022, **94**, 6902–6908.
20 M. Vacher, I. F. Galván, B.-W. Ding, S. Schramm, R. Berraud-Pache, P. Naumov, N. Ferré, Y.-J. Liu, I. Navizet, D. Roca-Sanjuán, W. J. Baader and R. Lindh, *Chem. Rev.*, 2018, **118**, 6927–6974.
21 G.-S. Zheng, C.-L. Shen, Q. Lou, J.-F. Han, Z.-Z. Ding, Y. Deng, M.-Y. Wu, K.-K. Liu, J.-H. Zang, L. Dong and C.-X. Shan, *Mater. Horiz.*, 2022, **9**, 2533–2541.
22 W. Zhou, S. Dong, Y. Lin and C. Lu, *Chem. Commun.*, 2017, **53**, 2122–2125.
23 M. J. Molaei, *Talanta*, 2019, **196**, 456–478.
24 L. Bao, C. Liu, Z. L. Zhang and D. W. Pang, *Adv. Mater.*, 2015, **27**, 1663–1667.
25 J.-W. Kang and D.-H. Kang, *Chem. Eng. J.*, 2021, **420**, 129990.
26 L. Đorđević, F. Arcudi, M. Cacioppo and M. Prato, *Nat. Nanotechnol.*, 2022, **17**, 112–130.
27 H. N. Kagalwala, J. Gerberich, C. J. Smith, R. P. Mason and A. R. Lippert, *Angew. Chem., Int. Ed.*, 2022, **61**, e202115704.
28 Y. Wang, Y. Bian, X. Chen and D. Su, *Chem. – Asian J.*, 2022, **17**, e202200018.
29 L. Delafresnaye, F. R. Bloesser, K. B. Kockler, C. W. Schmitt, I. M. Irshadeen and C. Barner-Kowollik, *Chem. – Eur. J.*, 2020, **26**, 114–127.
30 D. Chen, R. Peng, H. Zhou and H. Liu, *Microchim. Acta*, 2016, **183**, 1699–1704.

31 Z. Zhao, H. Zhang, J. W. Y. Lam and B. Z. Tang, *Angew. Chem., Int. Ed.*, 2020, **59**, 9888–9907.
32 P.-C. Yang, Y.-X. Ting, S. Gu, Y. Ashraf Gandomi, J. Li and C.-T. Hsieh, *Nanomaterials*, 2021, **11**, 1383.
33 G. Yu, Z. Sun, Y. Wu and N. Sai, *Spectrochim. Acta, Part A*, 2022, **268**, 120641.
34 M. Hesari and Z. Ding, *Nat. Protoc.*, 2021, **16**, 2109–2130.
35 K. Chu, J. R. Adsetts, J. Ma, C. Zhang, M. Hesari, L. Yang and Z. Ding, *J. Phys. Chem. C*, 2021, **125**, 22274–22282.
36 J. R. Adsetts, K. Chu, M. Hesari, Z. Whitworth, X. Qin, Z. Zhan and Z. Ding, *J. Phys. Chem. C*, 2022, **126**, 20155–20162.
37 A. Eghlimi, H. Jubaer, A. Surmiak and U. Bach, *J. Chem. Educ.*, 2019, **96**, 522–527.
38 S. Hu, A. Trinchi, P. Atkin and I. Cole, *Angew. Chem., Int. Ed.*, 2015, **54**, 2970–2974.
39 Z. Ding, B. M. Quinn, S. K. Haram, L. E. Pell, B. A. Korgel and A. J. Bard, *Science*, 2002, **296**, 1293–1397.
40 A. Bard, Z. Ding and N. Myung, *Struct. Bonding*, 2005, **118**, 1–57.
41 S. K. Lai, C. M. Luk, L. Tang, K. S. Teng and S. P. Lau, *Nanoscale*, 2015, **7**, 5338–5343.
42 M. M. Rauhut, L. J. Bollyky, B. G. Roberts, M. Loy, R. H. Whitman, A. V. Iannotta, A. M. Semsel and R. A. Clarke, *J. Am. Chem. Soc.*, 1967, **89**, 6515–6522.
43 M. Rauhut, D. Sheehan, R. Clarke, B. Roberts and A. Semsel, *J. Org. Chem.*, 1965, **30**, 3587–3592.
44 M. M. Rauhut, B. G. Roberts and A. M. Semsel, *J. Am. Chem. Soc.*, 1966, **88**, 3604–3617.
45 L. Wang, Z. Sofer and M. Pumera, *ACS Nano*, 2020, **14**, 21–25.
46 M. Park, I.-S. Choi and S.-Y. Ju, *Nanoscale Adv.*, 2022, **4**, 3537–3548.
47 M. M. Rauhut, A. M. Semsel and B. G. Roberts, *J. Org. Chem.*, 1966, **31**, 2431–2436.
48 Y. Ando, K. Niwa, N. Yamada, T. Irie, T. Enomoto, H. Kubota, Y. Ohmiya and H. Akiyama, *Photochem. Photobiol.*, 2007, **83**, 1205–1210.
49 B. Towaranonte and Y. Gao, *Anal. Lett.*, 2021, **55**, 186–202.
50 F. Kanoufi and N. Sojic, *Nature*, 2021, **596**, 194–195.